

05,06

## Features of the structure, microstructure, radio-emitting and radio-absorbing properties of mechanically and non-mechanically activated BiFeO<sub>3</sub> ceramics

© I.O. Krasniakova<sup>1</sup>, E.N. Sidorenko<sup>2</sup>, A.O. Galatova<sup>3</sup>, D.I. Rudsky<sup>3</sup>, E.V. Glazunova<sup>3</sup>, Yu.A. Kuprina<sup>3</sup>, A.V. Nazarenko<sup>4</sup>, N.B. Kofanova<sup>2</sup>, A.G. Rudskaya<sup>2,¶</sup>

<sup>1</sup>The Smart Materials Research Institute, Southern Federal University, Rostov-on-Don, Russia

<sup>2</sup>The Department of Physics, Southern Federal University, Rostov-on-Don, Russia

<sup>3</sup>Scientific Research Institute of Physics, Southern Federal University, Rostov-on-Don, Russia

<sup>4</sup>Southern Scientific Center, Russian Academy of Sciences, Rostov-on-Don, Russia

¶ E-mail: agrudskaya@sfedu.ru

Received December 28, 2022

Revised March 7, 2023

Accepted March 7, 2023

By the method of the two-stage solid-phase synthesis from a stoichiometric mixture of the bismuth and iron oxides, mechanically and non-mechanically activated samples of bismuth ferrite ceramics were prepared. The phase composition of the ceramic samples is predominantly BiFeO<sub>3</sub>, while Bi<sub>25</sub>FeO<sub>40</sub> and Bi<sub>2</sub>Fe<sub>4</sub>O<sub>9</sub> are recorded in minor amounts, the proportion of the latter decreases due to mechanical activation. Mechanical processing of the samples expands the range of linear sizes of microparticles. It has been established that mechanically activated bismuth ferrite ceramics absorb electromagnetic microwave energy up to –16 dB, while the samples of the original material absorb up to –25 dB. Both ceramic samples are capable of emitting a weak electromagnetic field, which decreases with increasing height above the sample.

**Keywords:** bismuth ferrite BiFeO<sub>3</sub>, solid-phase synthesis, mechanical activation, structure, microstructure, radio absorption and radio emission.

DOI: 10.21883/PSS.2023.04.55992.560

### 1. Introduction

In the rapidly changing modern world, the development of technique and technology is a topical challenge. One of key tasks in this direction is creation of new materials for many industries, such as engineering, construction, healthcare, etc. First of all, of interest are materials with unique properties: electric, magnetic, temperature-dependent, chemical properties, etc. Formation of such materials requires clear understanding of the relation between structural features of the substance (nanocrystalline structure, defectiveness, presence of amorphous, quasicrystalline or metastable phases, etc.) and presence of a certain unique property of the substance. In this case different kinds of impact can be used to modify the substance in the required direction, i.e. to create a material with required structural and, as a consequence, physical characteristics. This understanding of the relation between structure and physical properties of solid-phase substances gives the possibility of targeted design of materials with pre-defined properties. In this context, multifunctional materials seem to be promising, for example, bismuth ferrite. BiFeO<sub>3</sub> (BFO) is a multiferroic, i.e. it combines two of three

possible (mechanic, electric, magnetic) orders, namely, it simultaneously possesses ferroelectric and antiferromagnetic ordering at room temperature. In addition to multiferroic properties, bismuth ferrite has shown the presence of diode effect [1], photovoltaic effect [1–3], pyrocatalytic effect [4] and photocatalytic effect [5,6]. In addition, bismuth ferrite is chemically stable, non-toxic and characterized by relatively narrow band gap of  $\sim 2.2$  eV [7–11]. All the above-listed makes BiFeO<sub>3</sub> attractive for practical applications in modern, actively developing fields, such as magnetoelectricity, spintronics and photovoltaics. BiFeO<sub>3</sub> can be used to create sensors of magnetic field, information read/write devices and magnetic recording devices, high-precision equipment for work with microwave radiation and wireless energy transmission to miniature electronic devices.

As known, bismuth ferrite is at the boundary of stability of the perovskite structure [12], and in this context, as well as due to the narrow concentration interval of stability of the BiFeO<sub>3</sub> phase in the phase diagram of Bi<sub>2</sub>O<sub>3</sub>–Fe<sub>2</sub>O<sub>3</sub> [13], this substance is sensitive to thermodynamic conditions of preparation [14]. Problems of BiFeO<sub>3</sub> synthesis are regularly discussed in various modern publications. For example, in [15] the review of the results of various methods for

Structural and atomic parameters for BiFeO<sub>3</sub>, Bi<sub>25</sub>FeO<sub>40</sub> and Bi<sub>2</sub>Fe<sub>4</sub>O<sub>9</sub> compounds. Wyck — positions and multiplicity of atoms in the cell; *x*, *y* and *z* — atomic coordinates; SOF — site occupancy factor; *B* — thermal parameters of atoms [25–27]

Phase	Space-group symmetry, cell parameters	Atom	Wyck	<i>x</i>	<i>y</i>	<i>z</i>	SOF	<i>B</i> , Å <sup>2</sup>
BiFeO <sub>3</sub> [25]	R3c (№ 161) <i>a</i> <sub>H</sub> = 5.588(0) Å <i>c</i> <sub>H</sub> = 13.867(1) Å <i>V</i> = 374.9 Å <sup>3</sup> <i>Z</i> = 6	Bi	6a	0	0	0	1	0.5
		Fe	6a	0	0	0.2212(15)	1	0.8
		O	18b	0.443(2)	0.012(4)	0.9543(20)	1	0
Bi <sub>25</sub> FeO <sub>40</sub> [26]	I23 (№ 197) <i>a</i> = 10.184(0) Å <i>V</i> = 1056.1 Å <sup>3</sup> <i>Z</i> = 1	Bi1	24f	0.1763	0.3179	0.0139	1	0
		Fe1	2a	0	0	0	0.5	0
		Bi2	2a	0	0	0	0.5	0
		O1	24f	0.6487(7)	0.7465(8)	0.985(1)	1	0
		O2	8c	0.6841(7)	0.6841(7)	0.6841(7)	1	0
		O3	8c	0.8819(12)	0.8819(12)	0.8819(12)	1	0
Bi <sub>2</sub> Fe <sub>4</sub> O <sub>9</sub> [27]	Pbam (№ 55) <i>a</i> = 7.940(0) Å <i>b</i> = 8.440(0) Å <i>c</i> = 6.010(0) Å <i>V</i> = 402.8 Å <sup>3</sup> <i>Z</i> = 2	Bi1	4g	0.176	0.175	0	1	0.8
		Fe1	4h	0.349	0.333	0.500	1	0.8
		Fe2	4f	0	0.500	0.244	1	0.8
		O1	4g	0.140	0.435	0	1	0.8
		O2	8i	0.385	0.207	0.242	1	0.8
		O3	4h	0.133	0.427	0.500	1	0.8
		O4	2b	0	0	0.500	1	0.8

the synthesis of BiFeO<sub>3</sub> and a number of its solid solutions is given. Along with the most widespread method of solid-phase synthesis, wet methods of synthesis, such as synthesis from sol-gels, including synthesis by reactions in glycol gels, synthesis from solutions of polymer complexes, synthesis from metal complexes, synthesis by hydrothermal reactions find ever-growing applications. The following methods are applied as activators of chemical reactions: starting mechanochemical activation, microwave impacts, acoustic oscillations, oxidation reactions of burning, codeposition, sorption, etc. [16–22]. It is found, that pure perovskite phases of BiFeO<sub>3</sub> and its solid solutions are formed in a narrow temperature interval of (780 < *T* < 850°C). Usually, other phases are formed at other temperatures as well: Bi<sub>25</sub>FeO<sub>40</sub>, Bi<sub>46</sub>Fe<sub>2</sub>O<sub>72</sub>, Bi<sub>2</sub>Fe<sub>4</sub>O<sub>9</sub>, Bi<sub>24</sub>Fe<sub>2</sub>O<sub>39</sub>.

This study analyzes radio-emitting and radio-absorbing properties of ceramic samples of BiFeO<sub>3</sub> synthesized according to the standard ceramic technology from mechanically activated (MA) and non-mechanically activated (NMA) stoichiometric mixtures of bismuth oxide and iron oxide.

## 2. Experiment

### 2.1. Solid-phase synthesis

Ceramic samples of BiFeO<sub>3</sub> for the study were synthesized from Bi<sub>2</sub>O<sub>3</sub> and Fe<sub>2</sub>O<sub>3</sub> oxides of „analytically pure“ grade in a molar ratio of 1:1 according to the standard ceramic process using two-stage synthesis. At the first stage the mixture of input oxides was charged into the drum of a

AGO-2 ball mill with balls made of ZrO<sub>2</sub> with a diameter of 8 mm and a total weight of 200 g. Ethanol was added to the mixture as a dispersion medium and the mixture was atomized for 4 h. Rotation speed of the drums was 1820 rpm. Upon completion of the dispersion process, the content of drums was dried in a drying cabinet to evaporate alcohol. In the process of synthesis optimum modes of the first synthesis stage are set: *t*<sub>1</sub> = 850°C, 10 h [22]. Due to the fact that the first stage of synthesis results in formation of a „core–shell“ type product [23], the material was reblended before the second stage (synthesized pegs were milled) to provide better solid-phase reaction of the remaining precursors. Then the compound was sintered repeatedly at a temperature of *t*<sub>2</sub> = 850°C for 10 h [22].

To produce mechanically activated ceramic tablets, the synthesized powder was dispersed once again in ethanol for 15 min in the AGO-2 ball mill. Ceramic tablets were produced by powder pressing followed by baking.

### 2.2. X-ray diffraction analysis

The structural study was carried out at room temperature using an Ultima IV X-ray diffractometer by Rigaku, CuK<sub>α</sub>-radiation in the angular range of 10 ≤ 2θ ≤ 70° with a scanning step of 2θ = 0.02° and a scanning rate of 0.5 deg/min. This interval of 2θ angles was selected because it included the most intensive diffraction peaks. The extension of this interval toward 2θ ≥ 60° and 2θ ≤ 20° gives the possibility for the refinement taking into consideration the weak peaks of higher orders of reflections not only of the BiFeO<sub>3</sub> phase but also of the possible impurity

phases. At the same time a strong overlapping of these peaks is observed, which, of course, does not improve results of the refinement of structural parameters. The X-ray diffraction profiles were processed by the method of full-profile analysis using the Powder Cell software [24] and the PDWin 3.0 and the Inorganic Crystal Structure Database (ICSD) international crystallographic databases.

### 2.3. Microstructure

The microstructure of samples was studied on fresh cleavages of the ceramic materials at the Equipment Sharing Center of SSC of the RAS (<https://ckp-rf.ru/catalog/ckp/501994/>) using a Keyence VK-9700 optical 3D-scanning laser (408 nm) microscope and a Carl Zeiss EVO 40 scanning electron microscope (SEM). To record the effects of discharging and to improve quality of SEM recording, a conductive metal layer was applied before the analysis in a Quorum SC7620 magnetron sputter. However, the cleavages were not machined. Photos were obtained in the mode of high accelerating voltage and low current of the beam (EHT = 20 kV,  $I_{\text{probe}} = 20$  pA). Working distance was 8–9 mm.

### 2.4. Study of radio-absorbing and radio-emitting properties

Radio-absorbing properties were studied using a setup that included three interchangeable vibrational frequency generators (covering the range of 3.2–12 GHz), an indicator of standing-wave ratio (SWR) and attenuation, a wideband unbalanced microstrip line (MSL) as a measuring cell. The sample was placed on the cell surface in the region of central conductor. The MSL was operated in the travelling wave mode to determine energy loss in the sample. At the same time, an absorbing termination of 50 Ohm was connected to the MSL output to reduce reflection of the wave from the end of the waveguide line. The investigations were conducted at a room temperature without thermostating.

Emission spectra were obtained using rod-type or ring-type receiving antennas, a microwave diode and an indicator. A digital voltmeter was used as the indicator.

## 3. Results and discussions

To determine structural characteristics of the phases formed in the process of sample synthesis, models presented in the table were used.

Fragments of X-ray diffraction profiles of ceramic samples of mechanically activated and non-mechanically activated BiFeO<sub>3</sub> at room temperature are shown in Fig. 1. X-ray diffraction patterns of the input ceramic sample show all X-ray maxima typical for the BiFeO<sub>3</sub> with the perovskite structure. It can be seen, that, in addition to peaks corresponding to the main BFO phase, all X-ray diffraction patterns have peaks corresponding to impurity phases,

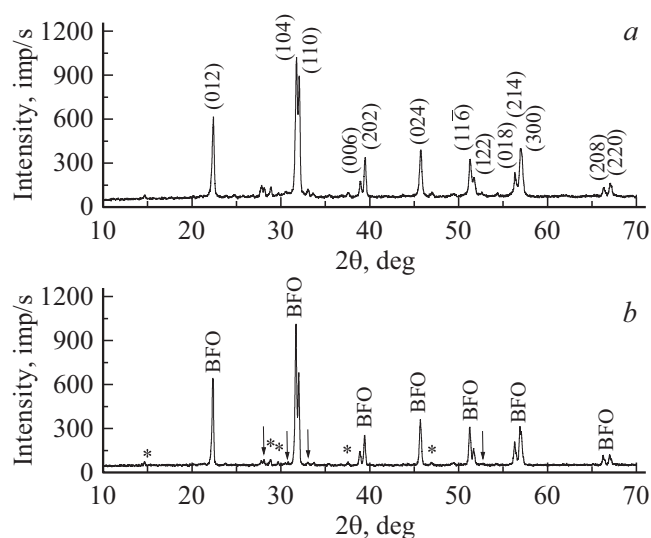


**Figure 1.** Fragments of X-ray diffraction profiles of BiFeO<sub>3</sub> ceramic samples (*a* — non-mechanically activated; *b* — mechanically activated) at room temperature. Miller indices for the BiFeO<sub>3</sub>-type phase are given for the R3c rhombohedral phase in hexagonal setting. (↓) and (\*) symbols denote X-ray diffraction reflections of the Bi<sub>25</sub>FeO<sub>40</sub> sillenite phase and Bi<sub>2</sub>Fe<sub>4</sub>O<sub>9</sub> mullite phase, respectively

namely the Bi<sub>25</sub>FeO<sub>40</sub> cubic phase of sillenite type and the Bi<sub>2</sub>Fe<sub>4</sub>O<sub>9</sub> orthorhombic phase with a structure of mullite type. That is, the solid-phase synthesis took place with the formation of impurity phases, which often occur during the bismuth ferrite production. The estimation based on the ratio of integral intensities of maximum intense reflections for each of the phases has shown that the percentage of sillenite is 4.7 and the percentage of mullite is 10.0% for NMA BFO and 2.5 and 6.5% for MA BFO, respectively. It is worth to note that mechanical activation decreases the number of impurity phases, at the same time the BFO structure remains rhombohedral with space group R3c and cell parameters  $a_{\text{H}} = 5.575(1)$  and  $c_{\text{H}} = 13.856(3)$  Å taken in the hexagonal setting. At the same time, narrowing is observed for reflections (012) by almost 1.5 times and for reflections (124) by 1.3 times, and, as a consequence, coherent scattering regions increase.

The analysis of microstructure of bismuth ferrite ceramic crystallites has shown that both the finely dispersed phase and the coarse grains present in both samples (Fig. 2). The sample without MA has fine grain sizes of  $\sim 0.5$  μm, coarse grain sizes of  $\sim 4$  μm, and the sizes are more or less uniform in their groups. The sample with MA has submicron grain sizes of up to 0.2–0.3 μm, and coarse grain sizes of up to 6–7 μm. Thus, there are differences in the sizes of crystallites against the background of extreme values.

Coarse crystallites have a regular shape that looks like a quadrangular prism. Fine grains have a round yet voluminous habit. This may be related to the fact that synthesis was running in the presence of a liquid phase.

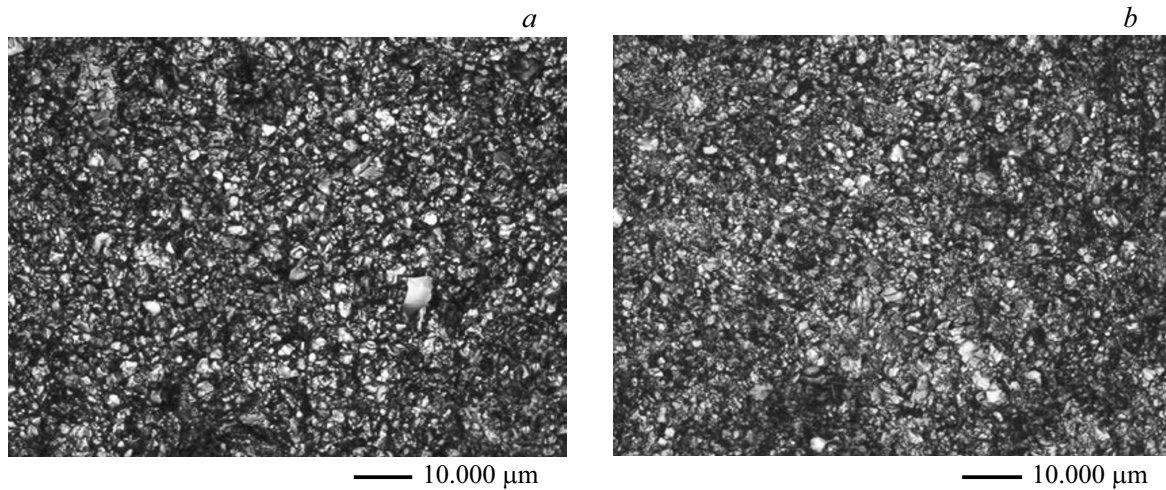


**Figure 2.** Microphotos of transverse cleavages of  $\text{BiFeO}_3$  ceramic samples with mechanical activation (*b*) and without it (*a*) (according to the data of optical microscopy).

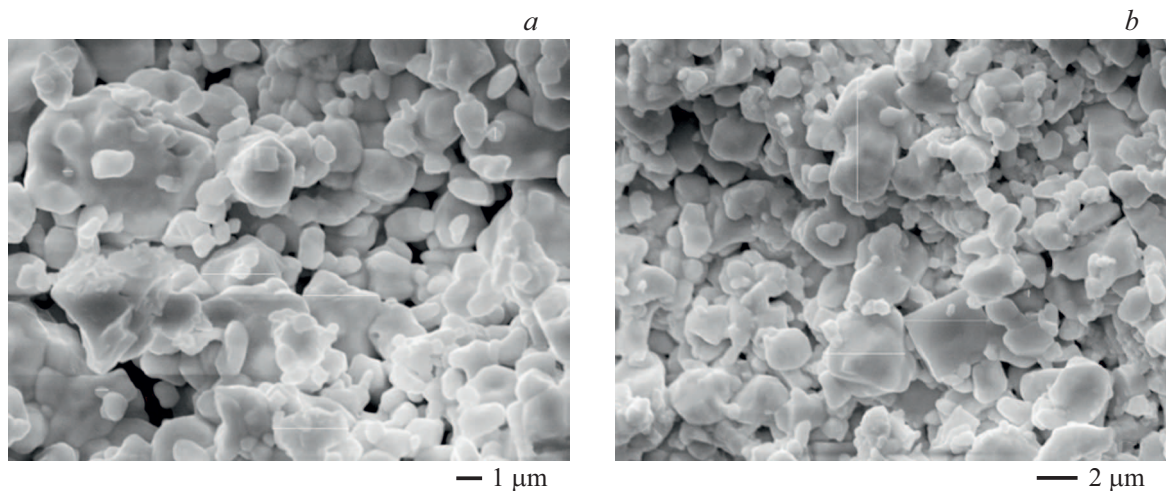


**Figure 3.** Microphoto of the  $\text{BiFeO}_3$  ceramic surface: *a* — without MA, *b* — MA sample (according to the data of SEM).

Its presence can be indirectly confirmed by visual examination as well: round edges of grains and the presence of conglomerates with „blurred“ boundaries. This effect is to a greater extent attributed to samples with MA. In samples without MA, grain boundaries are mainly observed.

The SEM data (Fig. 3) confirms the results of optical measurements of bismuth ferrite ceramics: the shape of bigger microparticles is closer to a regular geometry, fine particles are rounded to a greater extent. Sizes of particles of the NMA sample are within the range from 0.44 to 3.33  $\mu\text{m}$ , and those for the MA sample are in the range of 0.26–6.13  $\mu\text{m}$ . This is also consistent qualitatively with the optical distribution over sizes: the mechanical activation results in extension of the range of linear sizes of microparticles.

Measurements of electric component of the electromagnetic field near the NMA sample of  $\text{BiFeO}_3$  ceramic located on the MSL have shown that there is a weak emission field

above it that decreases as the distance from the sample surface to antenna increases (Fig. 4, *a*). Two emission regions have been found in the emission spectra of electric field in the range of 4.8–5.8 GHz with their peaks at  $\sim 5.3$  and  $\sim 5.7$  GHz, with a higher field intensity in the high-frequency region.

Also, emission spectra of magnetic component of the electromagnetic field (Fig. 4, *b*) demonstrate the presence of field above the sample surface and of two-mode type in the regions of 4.2–4.8 and 4.8–5.4 GHz with emission peaks at  $\sim 4.3$  and  $\sim 5.3$  GHz. There is no electromagnetic emission at frequencies higher than those mentioned above. The emission intensity decreases as the height increases, and this drop is more explicit in the region of higher frequencies down to complete disappearance of the field starting from  $h = 4.5$  mm.

Emission spectra for the mechanically activated sample of  $\text{BiFeO}_3$  ceramic, as well as for the sample without

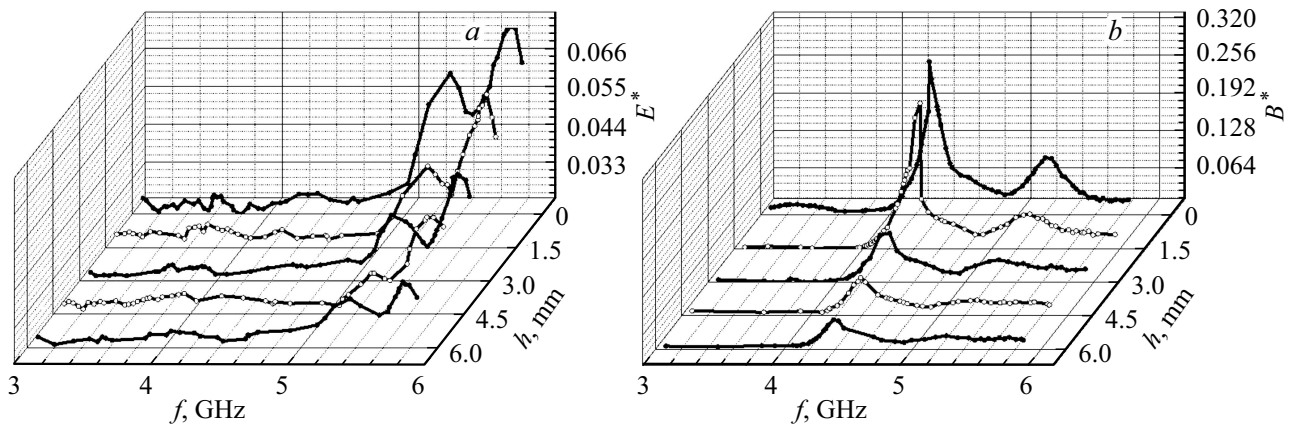


**Figure 4.** Emission spectra of electric  $E^*$  (a) and magnetic  $B^*$  (b) components of the electromagnetic field depending on the distance  $h$  to the surface of the NMA sample of  $\text{BiFeO}_3$  ceramic.

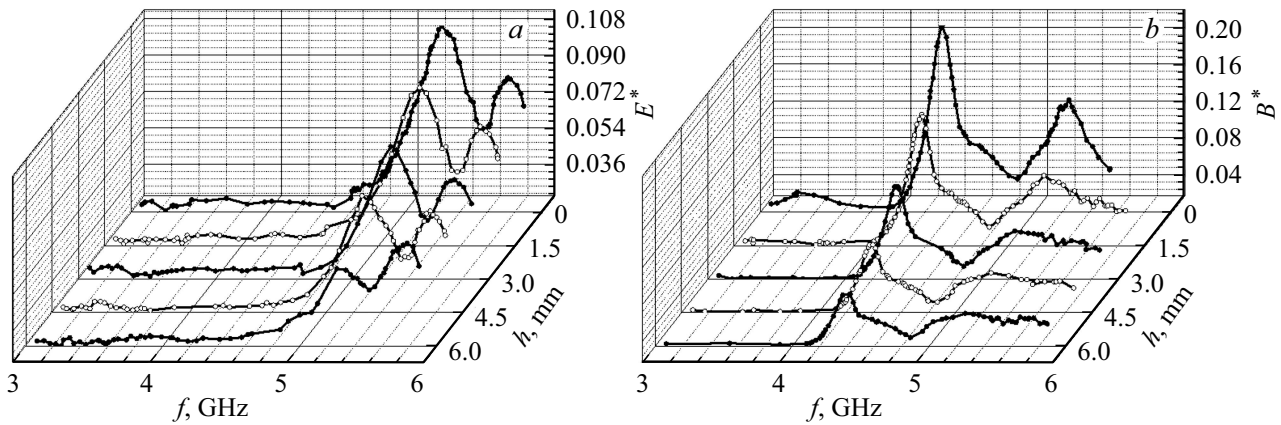


**Figure 5.** Emission spectra of electric  $E^*$  (a) and magnetic  $B^*$  (b) components of the electromagnetic field depending on the distance  $h$  to the surface of the MA sample of  $\text{BiFeO}_3$  ceramic.

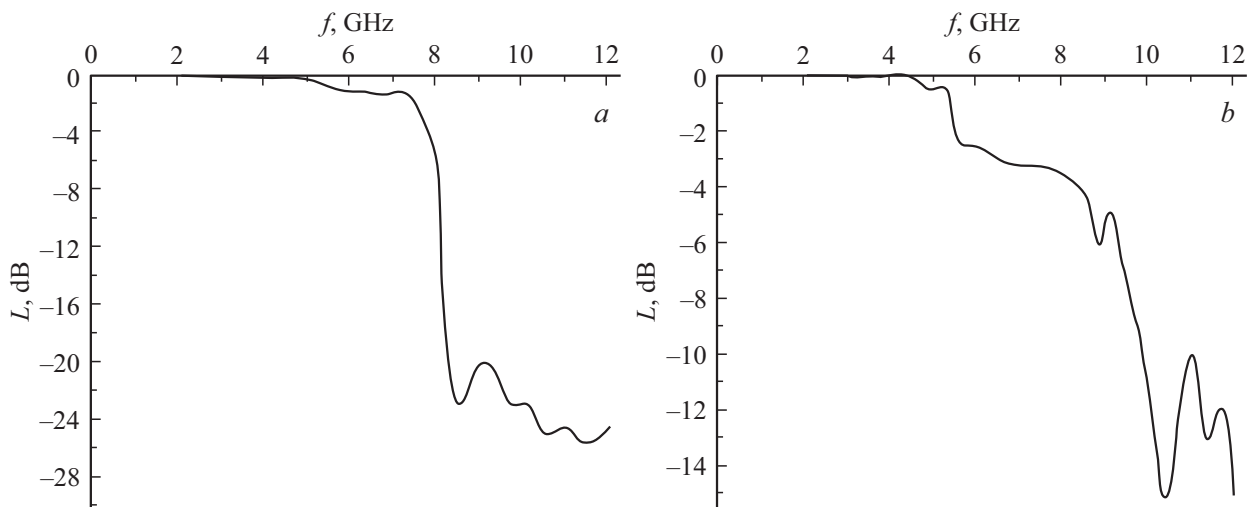


**Figure 6.** Spectra of electromagnetic field absorption by  $\text{BiFeO}_3$  ceramic samples:  $a$  — without mechanical activation,  $b$  — with mechanical activation.

MA, remain of two-mode type for both the electric field strength (Fig. 5, *a*) and the magnetic induction (Fig. 5, *b*). Peaks of  $E^*(f)$  and  $B^*(f)$  dependencies are also at approximately 5.3, 5.7 GHz and 4.3, 5.3 GHz, respectively, i.e. mechanical activation of the ceramics does not result in offset of peaks of the absorption bands. The profile of spectra varies to some extent: maximum intensity of emission on the  $E^*(f)$  graph is in the low-frequency region, and high-frequency component of magnetic field does not disappear even at heights of up to 6 mm.

Thus, the considered spectra are indicative of the fact the energy part absorbed by samples of BiFeO<sub>3</sub> ceramic is transformed to the energy of electromagnetic emission.

Fig. 6 shows absorption spectra of non-mechanically activated and mechanically activated samples of bismuth ferrite ceramics.

The analysis of spectra shows that in the region below ~ 7.5 GHz the absorption of microwave energy by the samples is nearly zero (0–2 dB). At higher frequencies a considerable energy absorption is observed in the range of up to 12 GHz. Absorption peaks are observed in the spectra, and the input, not mechanically activated, ceramics absorbs energy to a greater extent (up to –25 dB), than the ceramics without mechanical activation (up to –16 dB). The absorption profile varies to some extent as well: the level of absorption for the input ceramics varies slightly, however, in the case of mechanically activated ceramics more sharp fluctuations are observed. The shape of absorption spectrum of the input ceramics is determined likely by relaxation processes. More sharp peaks in the spectrum of the mechanically activated sample are probably indicative of resonance mechanism of the energy absorption.

#### 4. Conclusion

The method of two-stage solid-phase synthesis is used to prepare ceramic samples of BiFeO<sub>3</sub> with optimum process parameters  $t_1 = t_2 = 850^\circ\text{C}$ ,  $\tau_1 = \tau_2 = 10$  h. By the X-ray diffraction analysis it is shown, that the bismuth ferrite ceramics is inhomogeneous: its main phase is BiFeO<sub>3</sub>, minor phases are Bi<sub>25</sub>FeO<sub>40</sub> and Bi<sub>2</sub>Fe<sub>4</sub>O<sub>9</sub>.

Mechanical activation results in a decrease in the number of impurity phases. The study of morphology of BiFeO<sub>3</sub> ceramic cleavages by methods of optical and electron microscopy has shown the presence of both the finely dispersed phase and the coarse grain phase. Large crystallites have a regular quad shape, while fine grains have more rounded shape with voluminous habit. The mechanically activated ceramic sample has wider range of microparticle distribution over sizes than the sample prepared without mechanical processing. The mechanically activated bismuth ferrite ceramics absorbs electromagnetic microwave energy to –16 dB, and samples of BFO without mechanical activation absorb it to –25 dB. Both ceramic samples can emit a weak electromagnetic field that decreases as the height above the sample grows.

#### Funding

The study was supported by the Scientific Project No. GZ0110/22-01-EP „Development of the fundamental basis for technologies of functional nanomaterial synthesis to create energy-efficient components for microelectronics and nanoelectronics, devices of sensorics, energy transformation devices and neuromorphic systems“ within the scope of the state assignment of the Ministry of Science and Higher Education of the Russian Federation.

#### Conflict of interest

The authors declare that they have no conflict of interest.

#### References

- [1] T. Choi, S. Lee, Y.J. Choi, V. Kiryukhin, S.-W. Cheong. *Science* **324**, 5923, 63 (2009).
- [2] S.Y. Yang, J. Seidel, S.J. Byrnes, P. Shafer, C.-H. Yang, M.D. Rossell, P. Yu, Y.-H. Chu, J.F. Scott, J.W. Ager, L.W. Martin, R. Ramesh. *Nature Nanotechnology* **5**, 2, 143 (2010).
- [3] A. Bhatnagar, A.R. Chaudhuri, Y.H. Kim, D. Hesse, M. Alexe. *Nature Commun.* **4**, 2835 (2013).
- [4] J. Wu, W. Mao, Z. Wu, X. Xu, H. You, A.X. Xue, Y. Jia. *Nanoscale* **8**, 13, 7343 (2016).
- [5] U.A. Joshi, J.S. Jang, P.H. Borse, J.S. Lee. *Appl. Phys. Lett.* **92**, 24, 242106 (2008).
- [6] Y. Hou, M. Miao, Y. Zhang, J. Zhu, H. Li. *Chem. Commun.* **47**, 7, 2089 (2011).
- [7] X. Wang, W. Mao, Q. Zhang, Q. Wang, Y. Zhu, J. Zhang, T. Yang, J. Yang, X. Li, W. Huang. *J. Alloys Comp.* **677**, 288 (2016).
- [8] L. Lu, M. Lv, G. Liu, X. Xu. *Appl. Surface Sci.* **391**, 535 (2017).
- [9] T. Soltani, B.-K. Lee. *Chem. Eng. J.* **306**, 204 (2016).
- [10] L. Wang, C.-G. Niu, Yi. Wang, Y. Wang, G.-M. Zeng. *Ceram. Int.* **42**, 16, 18605 (2016).
- [11] T. Tong, H. Zhang, J. Chen, D. Jin, J. Cheng. *Catalysis Commun.* **87**, 23 (2016).
- [12] E.G. Fesenko, *Semeistvo perovskita i segnetoelektrichestvo*, Atomizdat, M., (1972) 248 p. (in Russian).
- [13] O. Diéguez, O.E. González-Vázquez, J.C. Wojdel, J. Íñiguez. *Phys. Rev. B* **83**, 094105 (2011).
- [14] Kh.A. Sadykov, I.A. Verbenko, L.A. Reznichenko, A.G. Abubakarov, L.A. Shilkina, O.I. Razumovskaya, S.I. Dudkina, *Konstruktsii iz kompozitsionnykh materialov* **2**, 130, 50 (2013) (in Russian).
- [15] J. Silva, A. Reayes, H. Esparza, H. Camacho, L. Fuentes. *Integrated Ferroelectrics* **126**, 47 (2011).
- [16] J. Lu, L.J. Qiao, P.Z. Fu, Y.C. Wu. *J. Cryst. Growth* **318**, 936 (2011).
- [17] A.V. Egorysheva, V.D. Volodin, O.G. Ellert, N.N. Efimov, V.M. Skorikov, A.E. Baranchikov, V.M. Novotortsev. *Inorganic Mater.* **49**, 303 (2013).
- [18] A. Perejón, P.E. Sánchez-Jiménez, J.M. Criado, L.A. Pérez-Maqueda. *J. Phys. Chem. C* **118**, 26387 (2014).
- [19] A.G. Abubakarov, L.A. Shilkina, I.A. Verbenko, L.A. Reznichenko, S.I. Dudkina. *Izv. RAN. Ser. fiz.* **78**, 8, 940 (2014). (in Russian).

- [20] T.V. Krasnyakova, S.A. Yurchilo, V.V. Morenko, I.K. Nosolev, E.V. Glazunova, S.V. Khasbulatov, I.A. Verbenko, S.A. Mitchenko. *Kinetika i kataliz* **61**, 3, 359 (2020). (in Russian).
- [21] I. Dmitrenko, K. Abdulvakhidov, A. Soldatov, A. Kravtsova, Zh. Li, M. Sirota, P. Plyaka, B. Abdulvakhidov. *Appl. Phys. A* **128**, 1128 (2022).
- [22] E.V. Glazunova, S.V. Khasbulatov, L.A. Shilkina, I.A. Verbenko, L.A. Reznichenko, In the collection: *Geoenergetika* / eds. M.Sh. MintsaeV, NPP „Geosfera“, Grozny (2019), P. 236. (in Russian).
- [23] M.S. Bernardo, T. Jardiel, M. Peiteado, A.C. Caballero, M. Villegas. *J. Eur. Ceram. Soc.* **31**, 3047 (2011).
- [24] W. Kraus, G. Nolze. *J. Appl. Cryst.* **29**, 301 (1996).
- [25] J.M. Moreau, C. Michel, R. Gerson, W.J. James. *J. Phys. Chem. Solids (JPCSA)* **32**, 1315 (1971).
- [26] C.E. Infante, B. Carrasco. *Mater. Lett.* **4**, 4, 194 (1986).
- [27] A.G. Tutov, V.N. Markin, *Izv. AN SSSR. Neorgan. materialy* **6**, 2014 (1970). (in Russian).

*Translated by Y.Alekseev*